Fully-three-dimensional positron emission tomography

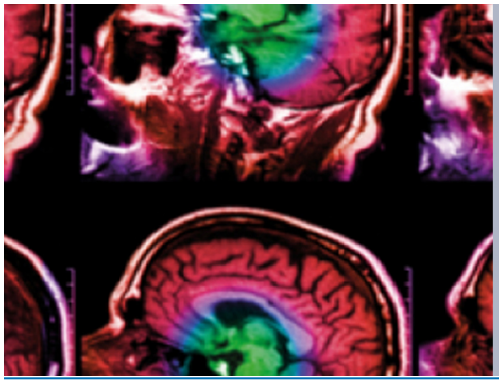

Phys. Med. Biol., 1980, Vol. 25. No. 1, 103–115. Printed in Great Britain

Fully three-dimensional positron emission tomography

James G Colsher†

Searle Radiographics, Des Plaines, IL 60018, USA

Received 26 January 1979, in final form 3 July 1979

Abstract. Fully three-dimensional positron emission tomography is considered and a reconstruction algorithm derived. The reconstruction problem is formulated mathematically as a three-dimensional convolution integral of a point spread function with an unknown positron activity distribution and is solved by Fourier transform methods. Performance of the algorithm is evaluated using both simulated phantom data produced by a Monte Carlo computer program and phantom data obtained from the University of Chicago/Searle Positron Camera. It is concluded that the method is computationally feasible and results in accurate reconstructions.

1. Introduction

During recent years considerable progress has been made in the development of computerised mathematical techniques for reconstruction of transverse section images (Budinger and Gullberg 1974, Gordon and Herman 1974). These techniques, often referred to as 'computerised tomography' and 'reconstruction from projections', usually involve reconstruction of a single transverse section at a time. When a three-dimensional reconstruction is required adjacent sections are reconstructed and the sections stacked. Such section-by-section reconstruction has been successful because (1) imaging systems can be designed so that the projection data lie in a single plane; and (2) reducing the three-dimensional problem to a series of two-dimensional problems greatly diminishes the mathematical and computational complexity. The simplification of mathematical calculations and the reduction of data arrays which results from the use of 2D-analysis allows the use of minicomputers.

Such section-by-section reconstruction is a useful process for positron imaging, but results in a low system sensitivity. Higher sensitivity positron imaging systems can be constructed and, in fact, are desirable since they can result in lowered radiation dose to the patient and shorter imaging times. However, for these systems the reconstruction problem can no longer be made two-dimensional so a three-dimensional technique is required.

This paper presents a mathematical algorithm for performing fully three-dimensional positron emission tomography. The reconstruction problem is formulated as the convolution of a point spread function with an unknown positron activity distribution. Fourier transform methods are used to derive the solution. This approach is shown to result in an algorithm which is only slightly more computationally complex than present day section-by-section algorithms. Performance of the algorithm is evaluated using both simulated phantom data produced by a Monte Carlo computer program and phantom data obtained from the University of Chicago/Searle Positron Camera.

† Present address: Cerebrovascular Research Center, Piersol Building, Hospital of the University of Pennsylvania, Philadelphia, PA 19104, USA

0031-9155/80/010103+13$01.00

2. The reconstruction problem

2.1. Background

A goal of nuclear medicine is the three-dimensional imaging of radionuclide activity distributions within the human body. Positron emission tomography, as discussed by Phelps (1977), Ter-Pogossian (1977) and Budinger *et al* (1977) represents one means of achieving this goal. The uniqueness of positron imaging results from the annihilation process which follows the emission of a positron from a nuclear transformation. The emitted positron will generally interact with an electron and produce two photons each with an energy of 511 keV. Conservation of momentum requires that these photons be emitted in nearly opposite directions (Colombino *et al* 1965). For the purpose of this paper it will be assumed that a positron–electron interaction will produce two back-to-back photons at the location of the emitter. If these two photons escape from the object and are detected by an imaging system, it can be inferred that the site of interaction must be somewhere along the ray defined by the detector loci.

A number of positron imaging systems capable of producing transverse section images have been developed. Although the details vary considerably, these systems generally consist of multiple detectors arranged in a ring and detect only coincidence events where the two back-to-back photons lie within the plane defined by the ring (Robertson *et al* 1973, Phelps *et al* 1975, Ter-Pogossian *et al* 1975, and Cho *et al* 1977). The data collected by such systems are processed using various reconstruction algorithms to obtain a single transverse section image. Multiple sections are obtained by translating the patient relative to the ring or by using a multiple ring system (Cho *et al* 1978, Ter-Pogossian *et al* 1978*a*, Ter-Pogossian *et al* 1978*b*). Adjacent sections are reconstructed and stacked to obtain a three-dimensional reconstruction. These systems suffer from low sensitivity since only a small fraction of the annihilation events will be detected.

An obvious method of increasing sensitivity is to increase the solid angle subtended by the detector system. This can be done by using a multiple ring system which detects interplane coincidence events in addition to the intraplane events or by rotating two opposed large-area detectors around the object to be imaged (Muehllehner *et al* 1977). As will be shown in the next section, inclusion of these interplane events requires a fully three-dimensional reconstruction algorithm. Given the theoretical results of Vainshtein and Orlov (1974) one can expect that reconstruction from this data is possible. The necessary data are certainly collected since the interplane events can be excluded and sequential transverse sections reconstructed from the intraplane data. Note that this situation differs from positron imaging with stationary large area detectors (Chu and Tam 1977) where all the theoretically required data are not obtained.

Although it is not the purpose of this paper to discuss the physics of positron imaging, there are some problems associated with accepting interplane events—namely the detection of undesired events. These arise from two sources. First, if one or both photons are scattered, their direction will change and the line connecting the detected event locations will not pass through the site of the emitter. Second and probably more important, are random coincidence events in which the two detected photons did not originate at the same site. As the geometrical sensitivity of a positron imaging system is increased, the ratio of undesired to true events will also increase. Good energy discrimination can to some extent eliminate the scatter coincidence events (Atkins 1978). The random coincidences can be controlled by using faster detectors and shorter

coincidence resolving time or by reducing the single-channel count rate. In practice there will be a trade-off between larger geometrical sensitivty and increased scatter and random coincidence fractions.

2.2. Mathematical formulation

In the general sense, the data obtained from any positron system consist of a set of rays in three-dimensional space which require processing to obtain an image. One processing procedure is to divide the image volume into volume elements (voxels) and back-project the rays through the volume. Each voxel along the ray path is incremented by a number proportional to the line length of the ray through the voxel. Alternatively the data can be sorted into two-dimensional projections (sets of parallel rays) which can then be back-projected through the volume, each voxel along the ray path being incremented by a number proportional to the projection value and the line length of the ray through the voxel. An estimate for the activity at a voxel is given by the weighted sum of all the rays passing through it. This procedure does not yield a true solution to the activity distribution but rather one that is blurred—the form of the blurring depending on the particular detector configuration and the set of rays that it detects.

To understand the nature of this blurring for any system detecting interplane events consider a point emitter located within the detector system (see figure 1). Rays within

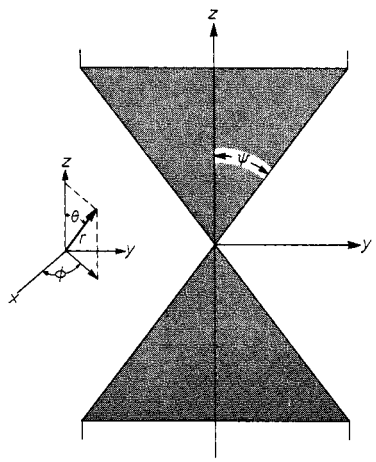

Figure 1. Cross-section of the point spread function. (Insert shows spherical coordinate system.)

the shaded region will be detected and back-projected to form the image of this point. In the limit where the number of detected events is large, this image, called the point spread function (PSF), has the following mathematical form

$$h(r, \theta, \phi) = \frac{1}{r^2} \operatorname{rect}_{\psi}\left(\theta - \frac{\pi}{2}\right) \tag{1}$$

where r, θ, ϕ are the coordinates in a spherical coordinate system and ψ is the acceptance angle of the detector system (Atkins *et al* 1977). The function $\operatorname{rect}_a(x)$ is equal to $1/2a$ for $|x| < a$ and is zero otherwise.

The PSF given above is for a point emitter located at the centre of the imaging system. If the point emitter is not located at the centre, the acceptance angle ψ is decreased (see figure 2). Restricting the acceptance angle for all points to the minimum value it can assume at any point makes the PSF independent of position. This spatial invariance of the PSF is a necessary condition in the mathematical development of section 3.

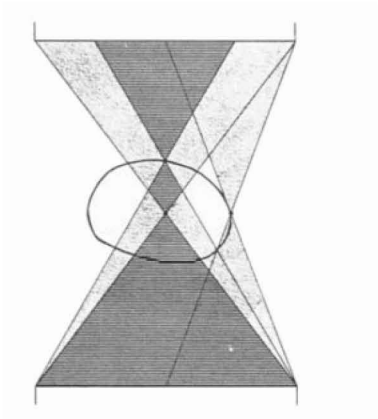

Figure 2. Variation of acceptance angle with source position.

For an arbitrary activity distribution $f(\boldsymbol{r})$, the back-projected image $g(\boldsymbol{r})$ is given by the three-dimensional convolution integral

$$g(\boldsymbol{r}) = \int f(\boldsymbol{r}')h(\boldsymbol{r}-\boldsymbol{r}')\,\mathrm{d}^3r' \tag{2}$$

where $\boldsymbol{r}$ is the spatial coordinate (r, θ, ϕ). Note that a convolution integral is appropriate only because the PSF $h(\boldsymbol{r})$ has been constrained to be spatially invariant. The reconstruction problem can now be simply stated in mathematicial terms. Given the back-projected image $g(\boldsymbol{r})$ and knowing the form for $h(\boldsymbol{r})$, determine the activity distribution $f(\boldsymbol{r})$. The general solution will be an inverse filter $h^{-1}(\boldsymbol{r})$ which can be convolved with the back-projected image $g(\boldsymbol{r})$ to oftain $f(\boldsymbol{r})$. The appropriate filter will be a three-dimensional function. Since the back-projection process is linear, it is also possible to filter the two-dimensional projections and then back-project the modified projections to obtain $f(\boldsymbol{r})$. In this case the appropriate filters will be a series of two-dimensional functions, one for each projection. The projection theorem (Budinger 1975) dictates that the two-dimensional filters will be slices or sections of the three-dimensional filter. This point will be addressed in more detail in the following section.

3. Reconstruction algorithm

Derivation of the reconstruction algorithm requires inversion of the integral equation given above (equation (2)) to develop an expression for $f(\boldsymbol{r})$ in terms of the known quantities $g(\boldsymbol{r})$ and $h(\boldsymbol{r})$. Taking the Fourier transform of both sides of equation (2) gives

$$G(\boldsymbol{s}) = F(\boldsymbol{s})H(\boldsymbol{s}) \tag{3}$$

where G, F, and H are the Fourier transforms g, f, and h respectively. $\boldsymbol{s}$ represents the

3D-cordinate in Fourier space (s, Θ, Φ). The Fourier transform is defined by

$$G(\boldsymbol{s}) = \int g(\boldsymbol{r}) \exp(2\pi i \boldsymbol{s}.\boldsymbol{r})\, \mathrm{d}^3 r. \tag{4}$$

The solution is

$$F(\boldsymbol{s}) = G(\boldsymbol{s})/H(\boldsymbol{s}) = G(\boldsymbol{s})H^{-1}(\boldsymbol{s}) \tag{5}$$

and the activity distribution is obtained by taking the inverse Fourier transform

$$f(\boldsymbol{r}) = \int F(\boldsymbol{s}) \exp(-2\pi i \boldsymbol{s}.\boldsymbol{r})\, \mathrm{d}^3 s. \tag{6}$$

This solution is straightforward provided the inverse filter $H^{-1}(\boldsymbol{s})$ can be determined and provided the filter is finite for all values of $\boldsymbol{s}$ where $F(\boldsymbol{s})$ exists.

3.1. Derivation of the filter

In this section an analytic expression for the filter $H^{-1}(\boldsymbol{s})$ is derived. The filter could be calculated from $h(\boldsymbol{r})$ using a numerical procedure (Chu and Tam 1977) however an analytic expression is preferable, because it allows easier examination of the properties of the filter. Since the PSF is circularly symmetric, the following form for the Fourier transform can be used (Bracewell 1965),

$$H(s, \Theta) = 2\pi \int_0^\infty \int_0^\pi h(r, \theta) \mathrm{J}_0(2\pi s r \sin\Theta \sin\theta) \exp(-2\pi i s r \cos\Theta \cos\theta) r^2 \sin\theta \, \mathrm{d}r \, \mathrm{d}\theta. \tag{7}$$

Substituting for the PSF (see equation (1)) and changing the order of integration gives

$$H(s, \Theta) = \frac{\pi}{\psi} \int_{\pi/2-\psi}^{\pi/2+\psi} \left[\int_0^\infty \mathrm{J}_0(2\pi s r \sin\Theta \sin\theta) \exp(-2\pi i s r \cos\Theta \cos\theta)\, \mathrm{d}r \right] \sin\theta \, \mathrm{d}\theta \tag{8}$$

so that

$$H(s, \Theta) = \frac{1}{2\psi s} \int_{\pi/2-\psi}^{\pi/2+\psi} \frac{\sin\theta \, \mathrm{d}\theta}{(\sin^2\Theta \sin^2\theta - \cos^2\Theta \cos^2\theta)^{1/2}} \tag{9}$$

since

$$\int_0^\infty \mathrm{J}_0(at) e^{\mathrm{i}bt} \, \mathrm{d}t = \frac{1}{(a^2 - b^2)^{1/2}} \tag{10}$$

(Abramowitz and Segun 1968).

By using various trigonometric substitutions, the above expression may be reduced to

$$H(s, \Theta) = \frac{|\sin\psi|}{2\psi s} \int_{-\infty}^{\infty} \frac{\mathrm{rect}_{\sin\psi}(\sin\theta)\, \mathrm{d}\sin\theta}{(\sin^2\Theta - \sin^2\theta)^{1/2}}. \tag{11}$$

This may be integrated by parts to obtain

$$H(s, \Theta) = \frac{1}{2\psi s} \left\{ \arcsin \frac{\sin\psi}{|\sin\Theta|} - \arcsin \frac{-\sin\psi}{|\sin\Theta|} \right\}. \tag{12}$$

This expression can be further simplified by considering two distinct regions in Fourier space, $|\Theta| > \psi$ and $|\Theta| \leqslant \psi$.

Region I. $|\Theta| > \psi$

$$H(s, \Theta) = \frac{1}{\psi s} \arcsin \frac{\sin \psi}{|\sin \Theta|}. \tag{13}$$

Region II. $|\Theta| \leq \psi$

In this region the arc sin function is complex. Using $\arcsin Z = \frac{1}{2} \log i [Z \pm (Z^2 - 1)^{1/2}]$ yields

$$H(s, \Theta) = \frac{\pi}{2\psi s}. \tag{14}$$

Thus the Fourier transform of the PSF is

$$H(s, \Theta) = \begin{cases} \dfrac{1}{\psi s} \arcsin \dfrac{\sin \psi}{|\sin \Theta|} & |\Theta| > \psi \\ \dfrac{\pi}{2\psi s} & |\Theta| \leq \psi \end{cases} \tag{15}$$

and the filter is simply the reciprocal of this expression

$$H^{-1}(s, \Theta) = \begin{cases} \dfrac{\psi s}{\arcsin \dfrac{\sin \psi}{|\sin \Theta|}} & |\Theta| > \psi \\ \dfrac{2\psi s}{\pi} & |\Theta| \leq \psi. \end{cases} \tag{16}$$

The angular dependence of this function is given in figure 3 where $H^{-1}(s, \Theta)/s$ is plotted for several values of the acceptance angle ψ. The behaviour of the filter is also shown pictorially in figure 4 where cross-sections of the filter for various acceptance angles are displayed. Several points should be made about this function. $H^{-1}(s, \Theta)$ is finite for all finite values of s and hence, in principal at least $F(s)$ can be recovered by multiplying $G(s)$ by $H^{-1}(s, \Theta)$. The function is also continuous in Θ as can be seen by substituting

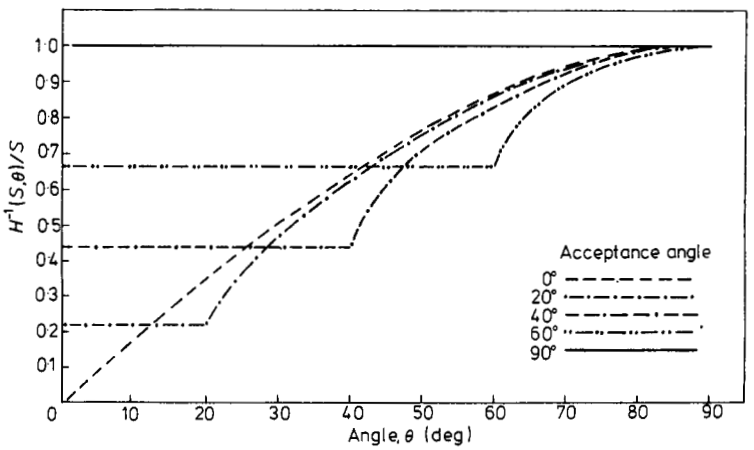

Figure 3. Angular dependence of the inverse filter. $H^{-1}(s, \Theta)/s$ is plotted for acceptance angles of 0°, 20°, 40°, 60°, and 90°.

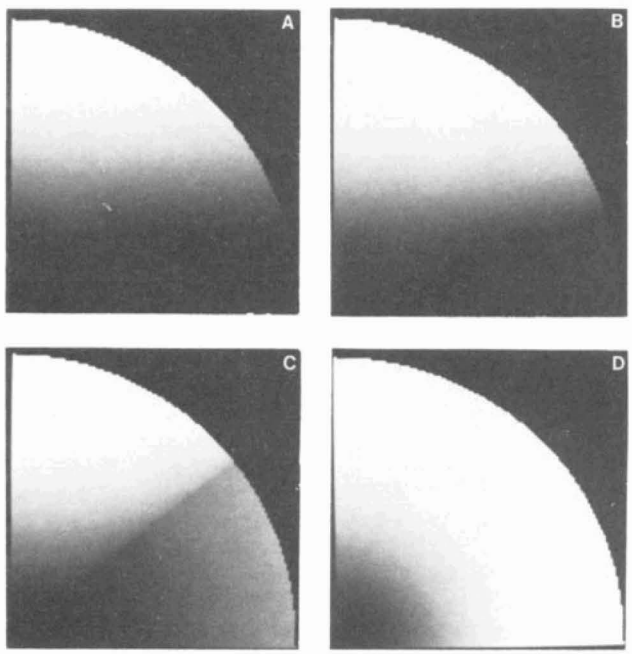

Figure 4. Cross-section of the inverse filter for various acceptance angles; A, 0°; B, 20°; C, 40°; and D, 90°. Because of symmetry only a single quadrant is shown for each angle.

$\Theta = \psi$ into equation 16 (also see figure 3). In the limiting case where $\psi = 0$ the expression reduces to a 'rho' filter and in the case where $\psi = \pi/2$ it reduces to an expression derived by Atkins *et al* (1977). This final point is discussed further in the next section.

The two-dimensional filter to be used for filtering the projections before back-projecting will be given by a cross-section of the three-dimensional filter. Due to symmetry the filter will be independent of the projection angle ϕ but will depend on the projection angle β and the maximum acceptance angle ψ. In fact it can be shown that

$$H_\beta^{-1}(\rho, \alpha) = \begin{cases} \dfrac{\psi\rho}{\arcsin \dfrac{\sin\psi}{(\sin^2\alpha + \cos^2\alpha \sin^2\beta)^{1/2}}} & |\sin^2\alpha + \cos^2\alpha \sin^2\beta| > \sin^2\psi \\ \dfrac{2\psi\rho}{\pi} & |\sin^2\alpha + \cos^2\alpha \sin^2\beta| \leqslant \sin^2\psi \end{cases} \tag{17}$$

where ρ and α are polar coordinates defined on the projection plane.

3.2. Limiting geometries

There are two limiting geometries for which the solution to the reconstruction problem is known. First, the case where $\psi = 0$ which corresponds to section-by-section geometry and second, the case where $\psi = \pi/2$, which corresponds to 4π geometry. The filter derived in the previous section should reduce to the filter for these two geometries when the appropriate value is substituted into equation (16).

Case I. $\psi = \phi$

When the acceptance angle is zero only annihilation events where the photons lie in a series of parallel sections will be detected. This case therefore corresponds to section-by-section reconstruction and the appropriate filter is the 'rho' filter (Bracewell and Riddle 1967, Budinger and Gullberg 1974).

For this case $|\sin\Theta| \geqslant \sin\psi = 0$ and the following formula applies

$$H^{-1}(s, \Theta) = \frac{\psi s}{\arcsin(\sin\psi/|\sin\Theta|)}. \tag{18}$$

This expression is indeterminate at $\psi = 0$; consequently one can use L'Hospital's rule to evaluate it.

$$H^{-1}(s, \Theta) = \lim_{\psi \to 0} \frac{\psi s}{\arcsin(\sin\psi/|\sin\Theta|)} = s|\sin\Theta|. \tag{19}$$

Note that $\rho = s|\sin\Theta|$ so the filter function reduces to the 'rho' filter as expected.

Case II. $\psi = \pi/2$ (90°)

When the acceptance angle is 90°, all the annihilation events can be detected. This, of course, does not represent a practical device since it corresponds to a spherical detection system or to infinitely large area-detectors. However it does provide another limiting case against which the solution for the filter can be compared.

For this case $|\sin\Theta| < \sin(\pi/2) = 1$ and therefore

$$H^{-1}(s, \Theta) = s \tag{20}$$

which agrees with the expression derived by Atkins *et al* (1977). As expected there is no Θ dependence.

3.3. Digital implementation

As with any numerical procedure, the image volume is divided into voxels and discrete Fourier transforms are used. Hence the continuous transforms of section 3.2 are replaced by discrete transforms with a finite cut-off. The assumption inherent to this procedure is that the functions involved, namely $F(s)$ and $G(s)$, are band-limited. Since any imaging system has a finite resolution this assumption is easily justified.

It is assumed that the three-dimensional back-projected image has already been calculated. The back-projection procedure has been discussed in some detail elsewhere (Muehllehner *et al* 1976, Atkins *et al* 1977) and only a brief summary will be given here. The reconstruction volume is divided into 16 transverse sections of 64×64 voxels. These values were determined by considering the resolution of the system used to acquire data and also the computer memory requirements (which in this case is an Interdata 8/32 with 384 kbytes of core memory). Each event is defined by the co-ordinates of the two detectors. The straight line connecting these coordinates represents the back-projected ray. On an event-by-event basis, the rays are traced through the volume and voxels along the ray path are appropriately incremented.

The first step in the reconstruction procedure is the calculation of the 3D-discrete Fourier transform of the back-projected image. In practice the back-projected image is extended from $64 \times 64 \times 16$ to $128 \times 128 \times 32$ by zero-filling the additional voxels and the transform of the $128 \times 128 \times 32$ image is calculated. This procedure avoids aliasing problems associated with performing discrete convolutions (Oppenheim and Schafer

1975). The next step is to multiply the transformed image by the inverse filter $H^{-1}(s, \Theta)$. Applying a sharp cut-off to the filter, i.e., simply truncating at some frequency, results in considerable oscillations in the reconstructed image (Chesler and Riederer 1975). This effect can be avoided if a modified filter is used. This modified filter is given by the product of $H^{-1}(s, \Theta)$ with a window function $W(s)$ chosen to make the cut-off of the Fourier transform relatively smooth. The window function used is the Hanning window (Blackman and Tukey 1958).

$$W(s) = \begin{cases} 0{\cdot}5 + 0{\cdot}5 \cos(\pi s / S_{\max}) & s \leqslant S_{\max} \\ 0 & s > S_{\max} \end{cases} \tag{21}$$

where $S_{\max}$ is the cut-off frequency. Other forms for the window function were also tried but reconstructions were found to be rather insensitive to the exact shape of the function, provided of course that a sharp cut-off was not used. Finally, the inverse 3D-Fourier transform of the $128 \times 128 \times 32$ matrix is calculated and $64 \times 64 \times 16$ reconstructed image is displayed.

4. Experimental evaluation

The performance of the algorithm was tested using computer-generated data and data obtained experimentally. The results are presented in this section.

4.1. Computer-generated data

The use of computer-generated data allows assessment of the performance of the algorithm independently of the imaging system. Assumptions inherent in the derivation of the algorithm, such as shift invariance of the PSF can be satisfied. Furthermore, it is easier to change the imaging conditions in a simulation since all that is usually involved are parameter changes and/or minor modifications to the existing computer program.

Computer-generated data were produced using Monte Carlo methods. An activity distribution was specified by defining centre locations in object space and distributions about the centre, either uniform or Gaussian. Event locations and direction cosines were generated randomly and the two back-to-back photons were then translated through space. If they struck the detectors, the coordinates at the detector were recorded on a list mode tape later to be back-projected into a three-dimensional volume. Constraints were placed on the acceptance angle to ensure uniform sensitivity and spatial invariance of the point spread function. The detector configuration consisted of two parallel square plates which were rotated about the object in 1° increments. Each detector was located equidistant from the centre of rotation. This configuration, rather than a multi-ring system, was chosen purely for convenience. Since the experimental data were obtained using a similarly configured system the list mode tape formats and processing procedures could be made identical. The phantom chosen is similar to that used by Chu and Tam (1977). It consisted of a 'skull region' corresponding to the blood supply for the brain, a 'brain' and a 'tumour'. The 'skull region' was a spherical shell 1·5 cm thick, with an inner diameter of 9 cm, an outer diameter of 10·5 cm, and relative activity of 1·0. The 'brain' was located inside the 'skull' and had a relative activity of 0·2. The 'tumour' was located off-centre with a radius of 1·8 cm and relative activity of 2·0.

Data were generated for two cases. In the first, the acceptance angle was 20° and in the second it was 40°. For each case more than two million events were detected and back-projected into a volume of $64 \times 64 \times 16$ voxels with a voxel size of $5 \times 5 \times 10$ mm. The back-projected and filtered images are shown in figure 5. The sections are displayed left to right and top to bottom so a three-dimensional object can be constructed by stacking the sections. Each group of sixteen images was scaled and displayed with 256 gray levels so the contrast varies depending on the maximum value.

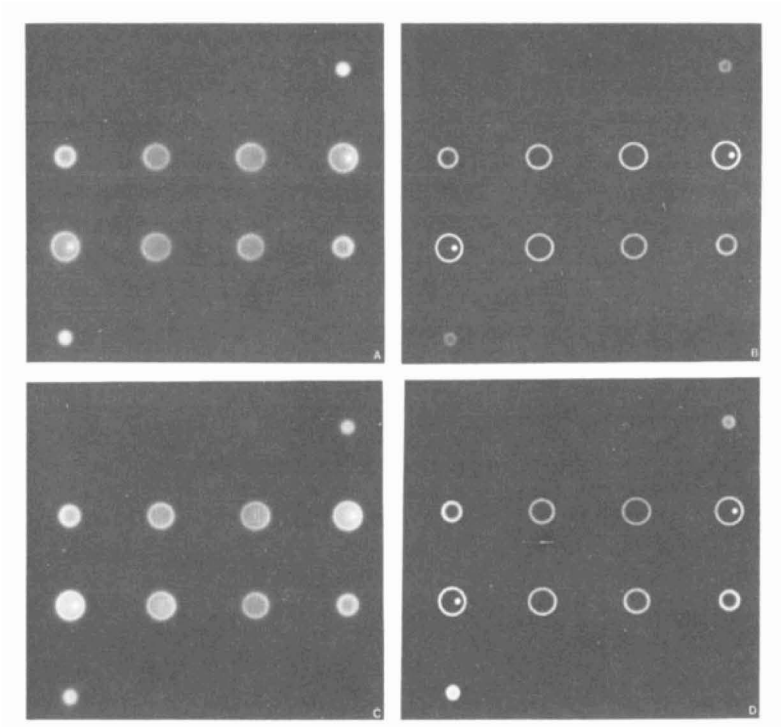

Figure 5. Reconstructions using computer generated data: A, back-projected image for 20° acceptance angle; B, filtered image for 20° acceptance angle; C, back-projected image for 40° acceptance angle; and D, filtered image for 40° acceptance angle.

The central section of the back-projected and filtered images is shown in figure 6. A histogram of the relative count densities along a line through the centre of the section is also shown. In the back-projected image the edges of the 'skull' are not clearly defined and the background 'brain' activity is considerably elevated. In the filtered image the edges are sharply delineated and the relative intensities of the various regions are approximately correct.

To ascertain the gain in geometrical sensitivity that fully 3D-reconstruction affords over section-by-section reconstruction, the data generated for the 40° acceptance angle was reprocessed by accepting events within: (a) a 40° acceptance angle; (b) a 20° acceptance angle; (c) sixteen 20 mm wide transverse sections; (d) sixteen 10 mm wide transverse sections. The ratio of counts is a measure of the relative sensitivity gain (see table 1). Note the substantial gains in sensitivity possible with fully 3D-reconstruction procedures.

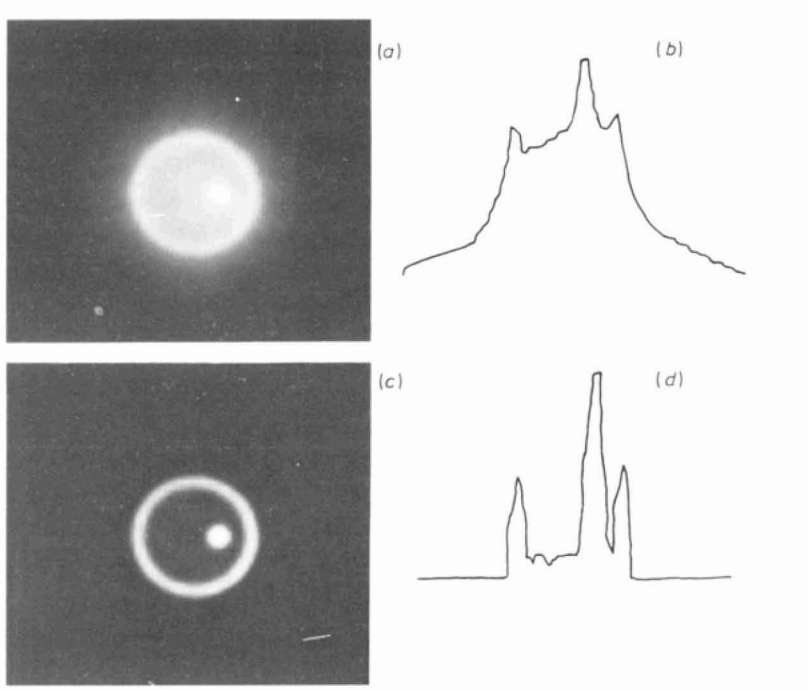

Figure 6. Single section of reconstruction using computer-generated data for 20° acceptance angle: (a) back-projected image; (b) histogram of central line through (a); (c) filtered image; (d) histogram of central line through (c).

Table 1. Gains in geometrical sensitivity.

Condition	Number of counts	Relative sensitivity† gain
3D-reconstruction		
40° acceptance angle	2158028	1270
20° acceptance angle	646931	380
Section-by-section reconstruction		
20 mm sections	6989	4
10 mm sections	1699	1

† Relative sensitivity is the ratio of number of counts for a particular condition to number of counts for 10 mm section condition.

4.2. Data obtained experimentally

Data obtained using the University of Chicago/Searle Positron camera were also processed using the algorithm. This camera has been described previously (Muehllehner *et al* 1976) and will not be discussed here except to note that the detectors are 37·5 cm in diameter and were adjusted so that they were 75 cm apart.

The phantom was a section of the Alderson body phantom (Alderson Research Laboratories, Stamford, Conn.). The radionuclide was ^{68}Ga-EDTA and the concentrations were adjusted as follows: body cavity = 1·3 Bq cm^{-3} (0·035 μCi cm^{-3}), liver = 13 Bq cm^{-3} (0·355 μCi cm^{-3}) and pancreas = 22 Bq cm^{-3} (0·595 μCi cm^{-3}). Over four

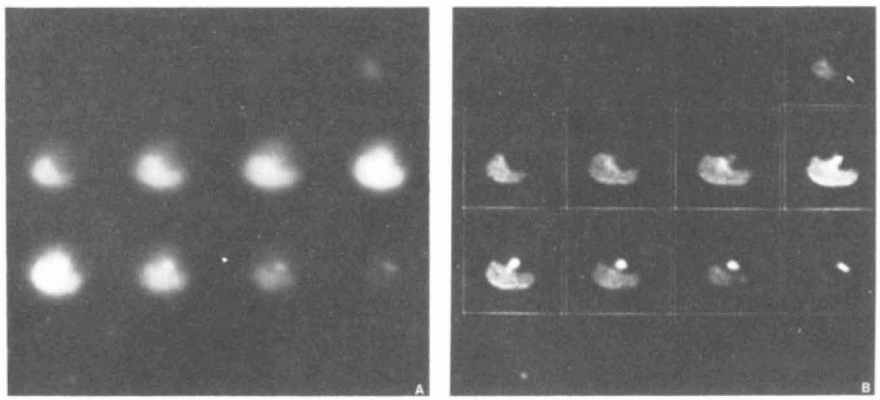

Figure 7. Reconstructions of experimental data: A, back-projected image; (B), filtered image.

million events were back-projected into $64 \times 64 \times 16$ voxels with a voxel size of $5{\cdot}8 \times 5{\cdot}8 \times 11{\cdot}6$ mm. The acceptance angle was limited to 20°. The back-projected and filtered images are shown in figure 7.

5. Conclusion

This paper considers several aspects of the problem of performing fully three-dimensional positron emission tomography. In particular, a mathematical algorithm for filtering the back-projected image or a series of two-dimensional projections is derived. The algorithm permits the use of interplane projection data in addition to intraplane data resulting in significant increases in the sensitivity of positron imaging systems.

A preliminary evaluation of the algorithm performance was conducted using both computer-generated and experimentally-obtained data. For the simple objects imaged accurate reconstructions with no serious artifacts were obtained. A more extensive evaluation to include an analysis of noise propagation and the effects of accidental coincidences and scatter coincidences in a large solid angle system should be considered.

Acknowledgments

I gratefully acknowledge the helpful advice and criticism provided by Dr Gerd Muehllehner, Department of Radiology, University of Pennsylvania, Philadelphia, PA, and I also thank Mr Joseph Dudek for obtaining the experimental data from the University of Chicago/Searle Positron Camera.

Résumé

Tomographie à émission de positrons à trois dimensions

L'auteur examine la tomographie à émission de positrons en trois dimensions en établissant un algorithme de reconstruction. Le problème de reconstruction est posé sous la forme d'un modèle mathématique et ainsi se ramène à l'intégrale de convolution tridimensionnelle d'une fonction de propagation d'un point comportant une distribution d'activité de positrons inconnue. Pour le résoudre on se sert des méthodes de transformation Fourrier. La valeur pratique de l'algorithme est évaluée en utilisant des données d'un fantôme de simulation mathématique engendré par le programme calculateur de Monte Carlo et en se servant des données d'un fantôme obtenues par la Caméra à Positrons de l'Université de Chicago/Searle. On arrive à la conclusion que la méthode est valable sur le plan calculateur et qu'elle permet des reconstructions précises.

Zusammenfassung

Vollständig dreidimensionale Tomographie mit Positronenausstrahlung

Betrachtet in diesem Beitrag wird die vollständig dreidimensionale Tomographie mit Positronenemission, indem ein Rekonstruktionsalgorithmus abgeleitet wird. Mathematisch wird das Rekonstruktionsproblem als dreidimensionales Konvolvier-integral einer Punktausweitungsfunktion mit einer unbekannten Positronenaktivitätsverteilung formuliert und mit Fourierschen Umwandlungsansätzen gelöst. Der interpretative Wert des Algorithmus wird anhand simulierter Phantomdaten, die mittels eines Monte Carlo-Rechnerprogramms erhalten worden sind, und mit Phantom-daten, die von der Positronenkamera in der Universität Chicago/Searle herrühren, ausgewertet. Als Schlußfolgerung wird festgestellt, daß die Methode rechnerisch durchführbar sei und zu genauen Rekonstruktionen führe.

References

Abramowitz M and Segun I A 1968 *Handbook of Mathematical Functions* (New York: Dover) p 487

Atkins F B 1978 *Ph.D. Thesis*, University of Chicago

Atkins F B, Muehllehner G and Harper P V 1977 in *Proc. 5th Int. Conf. on Information Processing in Medical Imaging, Nashville, Tennessee, 27 June–1 July 1977* (Oak Ridge National Laboratory, Tennessee, USA)

Blackman R B and Tukey J W 1958 *The Measurement of Power Spectra from the Point of View of Communications Engineering* (New York: Dover) p 98

Bohm, C, Eriksson L, Bergstrom M, Litton J, Sundman R and Singh M, 1978, *IEEE Trans. Nucl. Sci.* **NS-25** 624–37

Bracewell R 1965 *The Fourier Transform and Its Applications* (New York: McGraw Hill) pp 251–3

Bracewell R N and Riddle A C 1967 *Astrophys. J.* **150** 427–34

Budinger T F 1975 in *Technical Digest of Image Processing for 2-D and 3-D Reconstruction from Projections: Theory and Practice in Medicine and the Physical Sciences, Stanford, California, 4–7 August 1975* (Optical Society of America, Washington, DC)

Budinger T F, Derenzo S E, Gullberg G T, Greenberg W L and Huesman R H 1977 *J. Comput. Assist. Tomog.* **1** 131–45

Budinger T F and Gullberg G T 1974 *IEEE Trans. Nucl. Sci.* **NS-21** 2-20

Chesler D A and Riederer S J 1975 *Phys. Med. Biol.* **20** 632–6

Cho Z H, Eriksson L and Chan J 1977 in *Reconstruction Tomography in Diagnostic Radiology and Nuclear Medicine* ed. M M Ter-Pogossian *et al* (Baltimore: University Park Press) pp 393–421

Cho Z H, Nalcioglu O and Farukhi M R 1978 *IEEE Trans. Nucl. Sci.* **NS-25** 952–63

Colombino P, Fiscell B and Trossi L 1965 *Nuovo Cimento* **38** 707–23

Chu G and Tam K C 1977 *Phys. Med. Biol.* **22** 245–65

Gordon R and Herman G T 1974 *Int. Rev. Cytol.* **38** 111–51

Muehllehner G, Atkins F B and Harper P V 1977 in *Medical Radionuclide Imaging*, STI/PUB/440 Vol I (Vienna: IAEA) pp 391–407

Muehllehner G, Buchin M F and Dudek J H 1976 *IEEE Trans. Nuc. Sci.* **NS-23** 528–537

Mullani N A, Higgins C S, Hood J T and Currie C M 1978 *IEEE Trans. Nucl. Sci.* **NS-25** 180–3

Oppenheim A V and Schafer R W 1975 *Digital Signal Processing* (Englewood Cliffs: Prentice-Hall) pp 105–15

Phelps M E 1977 *Seminars in Nuclear Medicine* **7** 337–65

Phelps M E, Hoffman E J, Mullani N A and Ter-Pogossian M M 1975 *J. Nucl. Med.* **16** 210–24

Robertson J S, Marr R B, Rosenblum M, Radeka V and Yamamoto Y L 1973 in *Imaging in Nuclear Medicine* ed G S Freedman (New York: Society of Nuclear Medicine) pp 142–53

Ter-Pogossian M M 1977 *Seminars in Nuclear Medicine* **3** 109–27

Ter-Pogossian M M, Mullani N A, Hood J T, Higgins C S and Currie C M 1978a *Radiology* **128** 477–84

Ter-Pogossian M M, Mullani N A, Hood J T, Higgins C S and Ficke D C 1978b *J. Comput. Assist. Tomogr.* **2** 539–44

Ter-Pogossian M M, Phelps M E, Hoffmann E J and Mullani N A 1975 *Radiology* **14** 89–98

Vainshtein B K and Orlov S S 1974 in *Techniques of Three-Dimensional Reconstruction: Proc. Int. Workshop, Brookhaven National Laboratory, Upton, New York, 16–19 July 1974* (Brookhaven National Laboratory, Upton, NY, USA)